JOURNAL OF SOLID STATE CHEMISTRY 68, 193–213 (1987)

Computer Simulation of Transformations in Solids*

C. N. R. RAO† AND S. YASHONATH

Solid State and Structural Chemistry Unit, Indian Institute of Science, Bangalore 560 012, India

Received August 18, 1986

Recent developments in molecular dynamics (MD) and Monte Carlo (MC) methods enable us to fruitfully investigate transformations in solids by employing appropriate potentials. The possibility of varying both the volume and the shape of the simulation cell in these simulation techniques is especially noteworthy. In this article we briefly describe some of the highlights of the recent MD and MC methods and show how they are useful in the study of transitions in monatomic solids, ionic solids, molecular solids (especially orientationally disordered solids), and glasses. The availability of reliable pair potentials will undoubtedly make these methods more and more useful for studying various aspects of condensed matter in the years to come.

1. Introduction

Computer simulation is being used increasingly in diverse areas of science in the past few years. It has also emerged to become one of the powerful means for investigating condensed matter (*1*). The principal tools employed in computer simulation are the Monte Carlo and the molecular dynamics methods. In these methods, properties of a collection of particles, usually between 30 and 1000 in number, interacting via a potential $\phi(r)$ are obtained numerically. Reliable estimates of equilibrium and transport properties as well as microscopic properties can be obtained from such calculations.

In the Monte Carlo method, one performs stochastic averaging in the configuration space by means of the Metropolis importance sampling scheme (*2*). Monte Carlo calculations are generally performed in the canonical ensemble, the isothermal isobaric ensemble, or the grand canonical ensemble. In the canonical or the *NVT* ensemble calculations, the number of particles, N, the volume of the simulation cell, V, and the temperature, T, are constant during the course of the simulation. In isothermal isobaric or the *NPT* ensemble calculations, the number of particles, the pressure, P, and the temperature, T, are held constant. In the molecular dynamics method, Newton's equations of motion are solved numerically (*3*). The energy, E, of the system is conserved over the generated trajectory and the average of any property over this trajectory corresponds to the average in the microcanonical or the *NVE* ensemble.

There have been some significant advances in the methods of Monte Carlo and

* Contribution No. 356 from the Solid State and Structural Chemistry Unit.

† To whom all correspondence should be addressed.

0022-4596/87 $3.00

molecular dynamics in the last few years. The pioneering contribution of Andersen (*4*), provides a method for performing molecular dynamics calculations at constant pressure or constant temperature. The method enables the generation of trajectories corresponding to the isoenthalpic isobaric and isothermal isobaric ensembles. This is made possible by coupling the temperature and the pressure of the system to those of a bath. Another significant development is due to Parrinello and Rahman (*5*), who allowed for variation not only in the volume but also in the shape of the simulation cell in constant-pressure calculations. The modified molecular dynamics methods have been suitably employed by Nosé and Klein (*6*) for the study of polyatomic molecules. The Monte Carlo method has been modified by Yashonath and Rao (*7*) to include the variation in the shape of the simulation cell. These developments have rendered the molecular dynamics and the Monte Carlo methods most useful for the investigation of a variety of phenomena exhibited by condensed matter. The methods are important because they can be employed not only for the study of stable phases but also to examine systems undergoing transformations. The methods are therefore ideally suited to investigate microscopic as well as macroscopic changes accompanying phase transitions in solids.

In this article, we shall discuss studies of phase changes in solids carried out by the application of the generalized Monte Carlo and the molecular dynamics methods. This topic is of particular significance because of the recent modifications of the method to include both variation in size and shape of the simulation cell. What is especially gratifying is that we are now able to make meaningful predictions of phase transitions in real solids by employing reliable pair potentials. Besides phase transitions of molecular solids, we shall examine phase transitions in monatomic and ionic crystals. Some of the molecular systems discussed are CCl_4, CF_4, and adamantane. We shall present recent results on the glass transition obtained by the two methods, a noteworthy feature being the simulation of a real molecular glass formed by isopentane interacting via a realistic potential. The simulation study on isopentane glass has thrown some light on the structure of the glassy state. Andersen's cooling experiments on a Lennard-Jones fluid are also significant in this regard. We shall also indicate in the article the scope for further investigations of solids by computer simulation. Before discussing the various types of phase transitions of solids, we shall briefly review the recent developments in the Monte Carlo and molecular dynamics methods.

2. Recent Developments in Molecular Dynamics and Monte Carlo Methods

There are many excellent reviews on the standard molecular dynamics method dealing with calculations in the microcanonical ensemble as well as on the Monte Carlo method involving calculations in the canonical, isothermal isobaric, and grand canonical ensemble (*8*). In the present article, we shall limit ourselves exclusively to those developments that have taken place since the work of Andersen (*4*). In the molecular dynamics method, the developments are the constant-pressure, constant-temperature, constant-temperature–constant-pressure, variable shape simulation cell MD, and isostress calculations; in the Monte Carlo method, it is the variable shape simulation cell calculation.

2.1. Molecular Dynamics Methods

Constant-pressure calculations. In the traditional molecular dynamics calculations, the equations of motion for the coordinates $\mathbf{r}_1, \mathbf{r}_2, \ldots, \mathbf{r}_N$ of the N particles

confined to a cell of fixed volume V are solved numerically. This corresponds to constant volume and constant energy or the microcanonical ensemble. In the constant-pressure calculations, the volume is considered to be a dynamical variable in addition to these (*4*). The well-defined lagrangian

$$\alpha = \frac{1}{2}\sum_i m_i \dot{\mathbf{s}}_i \cdot \dot{\mathbf{s}}_i - \sum_{i<j} \phi(r_{ij}) + \frac{1}{2} M\dot{U}^2 - PU, \quad (1)$$

first utilized by Haile and Graben (*9*), is employed for the purpose. Here, m_i is the mass of the ith atom and the particle–particle interaction potential is denoted by $\phi(r)$. The scaled coordinate $\mathbf{s}_i$ of the ith particle and $\mathbf{r}_i$ are related by

$$\mathbf{s} = U^{1/3}\mathbf{r}. \quad (2)$$

If U is taken to be the volume V of the cell, the last two terms represent respectively the kinetic and the potential energies associated with motion of the simulation wall whose mass is M. The parameter P is the uniform hydrostatic external pressure acting on the simulation cell wall.

The lagrangian equations of motion

$$\frac{d}{dt}\left(\frac{\partial \alpha}{\partial \dot{x}}\right) = \frac{\partial \alpha}{\partial x}, \quad (3)$$

where x is a coordinate, are solved numerically to obtain the particle coordinate and momenta as a function of time t.

Andersen (*4*) has shown that the average of any function, F, over the trajectory thus generated is equal to the ensemble average for the isoenthalpic isobaric ensemble, i.e.,

$$\bar{f} = \bar{f}(N, P, H). \quad (4)$$

The enthalpy H is conserved over this trajectory and the external pressure corresponds to the value of P.

The value for the quantity M is chosen to approximately equal $U^{1/3}$ divided by the speed of sound in the system being simulated. Equilibrium properties of the system are independent of M and dynamical properties are dependent on M through the time scale of the volume fluctuations, the volume changes depending on the imbalance between the internal and the external pressure. The effect of M on single-particle dynamical properties seems to be small as indicated by the work of Nosé and Klein (*6*).

Constant-temperature calculations. Andersen (*4*) also proposed a constant-temperature method in which the energy fluctuates during the simulation. The lagrangian in this method is the same as that in the standard MD method. However, it differs from the standard MD method in that the particles undergo random stochastic collisions. The collisions are considered to be instantaneous and bring about a change in the momentum of the atom. The number of collisions and outcome of the collisions is determined by ν, the mean rate at which each particle suffers a collision and T the required temperature at which the simulation is to be performed. Particles are chosen randomly and a new value of momentum is assigned while the momentum and coordinate of all the other particles are unaltered. The new value for the momentum of the particle undergoing collision is chosen at random from the Boltzmann distribution corresponding to the temperature T of the simulation. The average of any property calculated from this trajectory equals the canonical ensemble average of that property for the specified values of (T, V, N) provided the Markov chain generated is irreducible (*4*). At low temperature and high densities, the Markov chain may not satisfy the irreducibility condition as in the traditional MD and MC techniques.

Equilibrium properties are independent of the value of ν, but the dynamical properties are not the same for two different values of ν. It is necessary to choose the value of ν within a small range (*10*). If the value is too high, the diffusion coefficient de-

creases, and if it is too small, large fluctuations occur in the kinetic energy and hence the temperature of the system. An appropriate choice for ν would be that resulting in a time for the decay of energy fluctuations approximately equal to that expected for a small volume of liquid in a large volume. Andersen (*4*) has discussed the method to estimate the optimum value of ν.

Nosé (*11*) has described another alternative formulation for performing calculations under constant-temperature conditions wherein an additional degree of freedom is introduced to permit energy fluctuations. The lagrangian for this system is given by

$$\alpha = \frac{1}{2}\sum_i m_i \dot{\mathbf{r}}^2 g^2 - \sum_{i<j} \phi(r_{ij}) + \frac{Q}{2}\dot{g}^2 - (f+1)kT_0 \ln g, \quad (5)$$

where the last two terms give the kinetic and potential energies associated with g, T_0 is the temperature at which simulation is carried out, and f is the number of degrees of freedom associated with N atoms. The velocities are scaled (*11*) as

$$\mathbf{v}_i = g\dot{\mathbf{r}}_i, \quad (6)$$

where $\mathbf{v}_i$ is the real velocity of particle i.

The physical system and the scaled system are related by Eq. (6). The scaling of velocities permits the exchange of heat between the simulated and the external heat reservoir. The equations of motion for the N atoms and the scaling factor g are solved numerically and averages calculated from the trajectory. The special choice $(f+1)kT_0 \ln g$ for the potential energy associated with g guarantees that the averages of equilibrium quantities calculated from the MD trajectory are the same as those in the canonical ensemble.

While Andersen's method for the constant-temperature calculation introduces energy fluctuations in the simulated system stochastically, Nosé's method achieves the same goal by the introduction of an additional degree of freedom; the scaling of velocities by a factor g can be interpreted as the scaling of time. This is similar to the scaling of coordinates in the constant-pressure method. The real time step $\Delta t'$ is given by

$$\Delta t' = \Delta t/g. \quad (7)$$

Thus, the real time steps, $\Delta t'$, are unequal in Nosé's formulation. As in constant-pressure calculations, the value of Q, in units of energy (time)^2, determines the dynamical quantities, although the equilibrium quantities are independent of the value of Q. The procedure for the selection of the optimum value for Q has been discussed by Nosé (*11*). It is believed that single-particle dynamics are less sensitive to the value of Q.

In the formulation of Nosé, the total hamiltonian, the total momentum, and total angular momentum are conserved. The conserved quantities help to monitor the precision of the calculation and also provide a powerful criterion to check for the correctness of the program.

Other methods for performing constant-temperature molecular dynamics calculations have been proposed recently. Evans (*12*) has introduced an external damping force in addition to the usual intermolecular force in order to keep the temperature constant in the simulation of a dissipative fluid flow. In another method, Haile and Gupta (*13*) have imposed the constraint of constant kinetic energy on the lagrangian equations of motion to perform calculations at constant temperature.

Constant-temperature–constant-pressure calculations. The trajectory for the atoms and volume are generated according to the solution of the equations of motion for the lagrangian (1) discussed earlier in connection with constant-pressure calculations. In addition, stochastic collisions are introduced to allow for fluctuations in en-

thalpy (*4*). The new momentum is sampled randomly from the Boltzmann distribution

$$\exp(-\boldsymbol{\pi}_i \cdot \boldsymbol{\pi}_i / 2m_i V^{2/3} kT), \qquad (8)$$

where $\boldsymbol{\pi}_i$ is the momentum conjugate to $\mathbf{s}_i$. The average over this trajectory obtained thus equals the ensemble average of the property in the isothermal isobaric ensemble.

Another MD formulation for constant-temperature and -pressure calculations based on the constant temperature formulation of Nosé (*11*) has been described recently. The stochastic collisions which permit energetic fluctuations has been replaced by the dynamic method of scaling of velocities of the atoms, in addition to the scaling of velocities by $V^{1/3}$. The method, which is completely dynamical, requires one to choose appropriate values for Q and M which respectively determine the time scale of the temperature and volume fluctuations.

Parrinello–Rahman method. The constant pressure MD formulation of Andersen (*4*) provides a method for permitting the variation in the volume of the simulation cell. Parrinello and Rahman (*5, 14, 15*) generalized Andersen's method to include variations in the volume as well as the shape of the simulation cell. In the Parrinello–Rahman formulation, the simulation cell is represented by three vectors, **a**, **b**, and **c**. The lagrangian is given by

$$\alpha = \frac{1}{2}\sum_{i}^{N} m_i \dot{\mathbf{s}}_i G \mathbf{s}_i - \sum_{i<j} \phi(r_{ij}) + \frac{1}{2} M \operatorname{Tr}(\mathbf{h}'\dot{\mathbf{h}}) - PV, \qquad (9)$$

where the simulation cell is represented by $\mathbf{h} = \{\mathbf{a}, \mathbf{b}, \mathbf{c}\}$ and the scaled coordinates by $\mathbf{s}_i = \mathbf{h}^{-1}\mathbf{r}_i$. The metric tensor $G = \mathbf{h}'\mathbf{h}$.

The external hydrostatic pressure on the system is denoted by P. The equations of motion are

$$\ddot{\mathbf{s}}_i = m_i^{-1} \sum_{i \neq j}^{N} \frac{1}{r_{ij}} \frac{d\phi(r_{ij})}{dr_{ij}} (\mathbf{s}_i - \mathbf{s}_j) - G^{-1}\dot{G}\dot{\mathbf{s}}_i, \quad i, j = 1, 2 \ldots N$$

$$\ddot{\mathbf{h}} = W^{-1}(\boldsymbol{\pi} - P)\boldsymbol{\sigma}, \qquad (10)$$

where $\boldsymbol{\sigma}_{ij} = \partial V / \partial h_{ij}$. The internal stress tensor $\boldsymbol{\pi}$ is given by

$$V\boldsymbol{\pi} = \sum_i m_i \mathbf{v}_i \mathbf{v}_i + \sum_{i<j} \frac{1}{r_{ij}} \frac{d\phi(r_{ij})}{dr_{ij}} (\mathbf{r}_i - \mathbf{r}_j)(\mathbf{r}_i - \mathbf{r}_j), \qquad (11)$$

the vector $\mathbf{v}_i$ being $\mathbf{h}\dot{\mathbf{s}}_i$. The imbalance between the internal stress $\boldsymbol{\pi}$ and the external pressure P acting on the cell wall given by $\boldsymbol{\sigma}$ determines the motion of the cell **h**. This method has been appropriately modified for calculations on molecular systems by Nosé and Klein (*6*).

Andersen's formulation is useful in the study of fluid–solid transitions where the change in volume is significant. The generalization of Parrinello and Rahman which allows variations in both the volume and the shape of the simulation cell is most suited for the study of phase transformations in solids. In the case where only the volume is allowed to change, the periodic boundary conditions do not permit the solid to undergo structural transformations involving a change in crystal symmetry. The variable shape MD method has been modified to include external stress rather than uniform hydrostatic pressure (*16*). A generalization to the isothermal isotension ensemble calculation giving a somewhat different interpretation of the additional degree of freedom introduced in the constant-temperature and -pressure formulation of Nosé has been discussed recently by Ray and Rahman (*17*).

2.2. *Modified Monte Carlo Method*

The traditional MC method in the isothermal isobaric ensemble has been modified to include variations in size as well as the shape of the simulation cell (*7*). The

average of any quantity, F, in the usual isothermal isobaric calculation is given by

$$F(\mathbf{r}^N, V) = \frac{\int_0^\infty dV \int_V d\mathbf{r}^N f(\mathbf{r}^N, V) \exp[-\beta\Phi(\mathbf{r}^N)]}{\int_0^\infty dV \int_V d\mathbf{r}^N \exp[-\beta\Phi(\mathbf{r}^N)]}, \quad (12)$$

where $\mathbf{r}_1, \mathbf{r}_2, \ldots, \mathbf{r}_N$ are the coordinates of the N atoms and are represented by $\mathbf{r}^N$, $\beta = 1/kT$, and Φ is the total potential energy. The simulation cell is a cube with edge length $L = V^{1/3}$. In order to allow both the size and shape of the cell to vary during the simulation, the cell is defined as in the Parrinello–Rahman MD method by the three vectors $\mathbf{a}$, $\mathbf{b}$, $\mathbf{c}$ (*7*). The matrix $\mathbf{h} = \{\bar{\mathbf{a}}, \bar{\mathbf{b}}, \bar{\mathbf{c}}\}$ represents the cell. For purposes of integration, the scaled coordinates $\boldsymbol{\alpha}_i = \mathbf{h}\mathbf{r}_i$ are employed rather than $\mathbf{r}_i$, where the components of $\boldsymbol{\alpha}_i$ vary between 0 and 1. The average of any quantity f in the modified isothermal isobaric ensemble is given by

$$f([\mathbf{h}\boldsymbol{\alpha}]^N, \mathbf{h}) = \frac{\int_0^\infty d\mathbf{h} \int_{\mathbf{h}} d[\mathbf{h}\boldsymbol{\alpha}]^N f([\mathbf{h}\boldsymbol{\alpha}]^N, \mathbf{h}) \exp(-\beta\Phi([\mathbf{h}\boldsymbol{\alpha}]^N, \mathbf{h}))}{\int_0^\infty d\mathbf{h} \int_{\mathbf{h}} d[\mathbf{h}\boldsymbol{\alpha}]^N \exp(-\beta\Phi([\mathbf{h}\boldsymbol{\alpha}]^N, \mathbf{h}))}. \quad (13)$$

A trial move is made by displacing the particle and also the cell edge:

$$\begin{aligned} \boldsymbol{\alpha}_i &\rightarrow \boldsymbol{\alpha}_i \pm \varepsilon_P \bar{\mathbf{R}} \\ \mathbf{a}_i &\rightarrow \mathbf{a}_i \pm \varepsilon_c \bar{\mathbf{A}}, \end{aligned} \quad (14)$$

where ε_P and ε_c are random numbers between 0 and 1 and $\bar{\mathbf{R}}$ and $\bar{\mathbf{A}}$ specify respectively the maximum particle and cell displacements.

It is noteworthy that Monte Carlo simulations involve simpler coding than molecular dynamics simulations. The Monte Carlo method therefore provides a convenient alternative to the molecular dynamics method if one is not interested in the dynamics of the system. In recent years many workers have felt the need for employing more complicated intermolecular potentials in order to predict accurately the properties of matter, especially those in the solid state. In such situations, the MC method is to be preferred as it is easier to code programs which incorporate complicated intermolecular potentials. Another advantage of the MC method is the ease with which the number of degrees of freedom can be altered in any calculation.

The above method is easily extended to perform calculations in isostress isothermal ensemble employing an isotropic stress tensor in place of a uniform hydrostatic pressure (*18*). The extension of the MC method to the case of polyatomic systems is straightforward (*19*). In the case of molecular systems, however, there are instances where the simulation cell rotates as a whole in space. For example, in the simulation of the low-temperature, high-pressure phase of carbon tetrachloride carried out by us, the simulation cell rotated in space (*19*). The variation of the magnitudes of $\mathbf{a}$, $\mathbf{b}$, and $\mathbf{c}$ and angles α, β, and γ of the simulation cell, as well as the variation of the cell components, is shown in Fig. 1. It is apparent from the figure that while the cell components change continuously during the course of a run, the magnitudes and angles of the vectors fluctuate around their average values. Similar rotation has been observed in a molecular dynamics study of the high-pressure phase of nitrogen by Nosé and Klein (*6*). Only six degrees of freedom are required (a, b, c, α, β, and γ) to define the cell. The rotation is a consequence of the three extra degrees of freedom associated with the simulation cell. The cell can be prevented from rotating by imposing a restriction on the cell so as to allow six degrees of freedom to be varied (*19*). Nosé and Klein (*6*) have proposed a method wherein the system is rotated to keep the

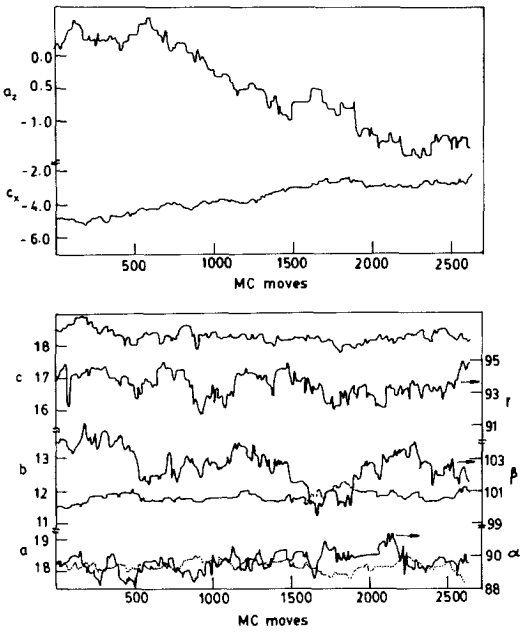

FIG. 1. Variation of the cell components c_x and a_z, the cell edges a, b, and c, and angles α, β, and γ during the first 2500 MC moves in the simulation of carbon tetrachloride, indicating the rotation of the cell. Angles are in degrees and the lengths in Å. (From Yashonath and Rao (*19*).)

growth of the antisymmetric component to zero after each step. While both methods can be used in the simulation of polyatomic systems, the former has the advantage that it is simpler to implement and also requires significantly less computer time.

2.3. General Remarks Regarding the MD and MC Methods

The MC and MD methods permitting the variation of the shape of the cell are best suited for the study of phase transitions in solids. These methods have been used to study phase transitions of a few solids in the last few years. Among these are monatomic solids such as rare gas solids, ionic solids, and molecular solids. There are, however, some inherent limitations in these methods. While certain transitions are readily investigated by these methods, others are more difficult. The b.c.c. to f.c.c. transformation of monatomic solids is an example of a transition that is readily observed (*5*, *7*) (see Figs. 2 and 3). This transition has been observed as a function

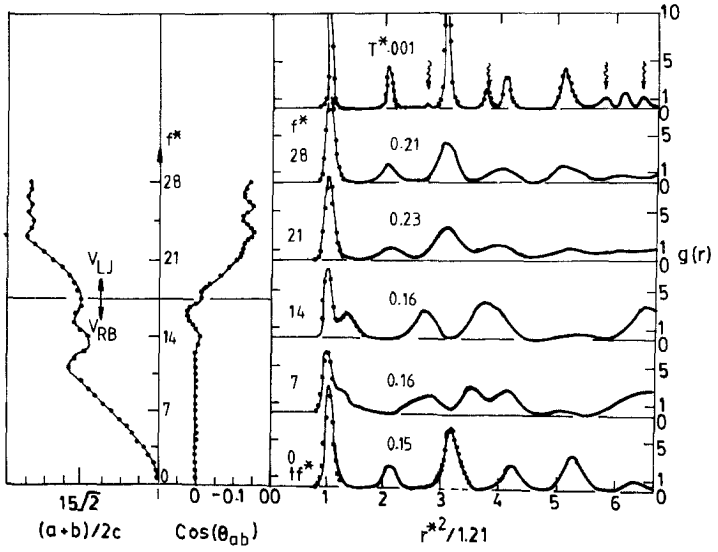

FIG. 2. Variation of the ratio $(a + b)/2c$ and cos θ_{ab} (left), where θ_{ab} is the angle between the cell edges a and b, and the r.d.f.'s at various times (right) from the MD study of Parrinello and Rahman (*5*), showing the transition from f.c.c. to b.c.c. and from b.c.c. to f.c.c. due to a change of interaction potential between the particles.

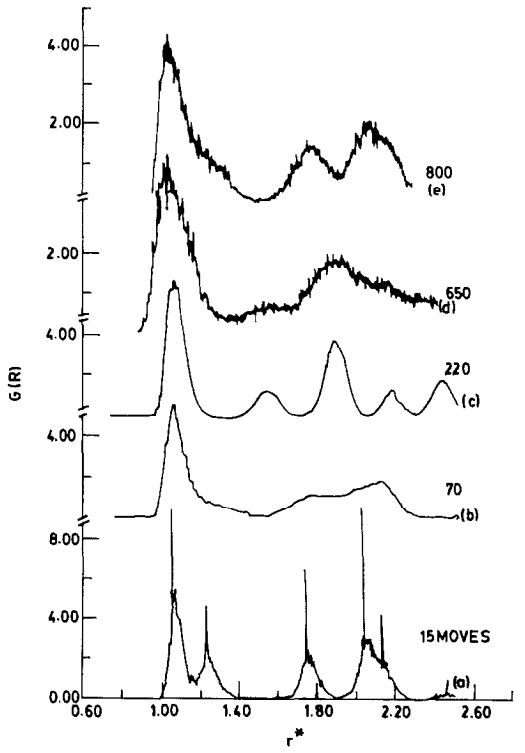

FIG. 3. Pair correlation functions as functions of reduced distance r^*. The b.c.c. arrangement transforms to f.c.c. at 220 MC moves when the Lennard-Jones potential is employed. If at this stage the interaction is changed to cesium potential, there is a change back to the b.c.c. at 450 MC moves. (From Yashonath and Rao (*7*).)

of pressure in helium and also on changing the interaction potential from that for cesium or rubidium to the Lennard-Jones potential. The transition from h.c.p. to f.c.c. is an example of a difficult transition. This transition requires a modification at the fourth shell of neighbors and both MD and MC calculations have failed to simulate the transformation (*20, 21*). There are also limitations imposed by the use of periodic boundary conditions and finite size effects (*22*).

In spite of the aforementioned limitations, the MD and MC methods can be most profitably employed in the investigations of a variety of systems. These methods provide fairly good approximations to average properties even when a relatively small number of particles (30 to 1000) are employed and are computationally quite economical. This is in contrast to the alternative method described in the literature (*22, 23*) which requires expensive hardware, considerable memory, and computer time, as it requires a much larger number of particles for the same accuracy. This method, however, has the advantage of being relatively free from effects due to finite size and periodic boundary conditions.

Calculations carried out by us (*7*) by the MC method where only the nine degrees of freedom were permitted and no particle displacements were allowed could successfully reproduce the f.c.c. to b.c.c. transition (Fig. 3). These and other considerations suggest that the MC method is to be preferred to the MD when only the equilibrium properties are of interest. For example, if one is interested in the determination of a phase diagram, the MC method would be more appropriate than the MD method. The MD method is preferable for obtaining dynamic properties even though it is not clear how one can obtain the exact dynamical behavior (*4, 6*). The technical details and aspects of programming for the MD and the MC methods are available (*6, 21*) and we shall not discuss them here.

3. Applications of MD and MC Methods to the Study of Transformations in Crystals

3.1. Monatomic Solids

Parrinello and Rahman (*5*) in their MD study investigated the relation between structure and interaction potential by employing two different potentials. The (6–12) Lennard-Jones potential which predicts the f.c.c. arrangement as the stable structure and the rubidium potential which has the stable b.c.c. structure were employed for

the purpose. Starting with a f.c.c. structure, they found that the solid transformed to a b.c.c. structure on changing the particle interaction from the Lennard-Jones to the rubidium potential. The radial distribution functions (r.d.f.'s) show distinct peaks corresponding to a b.c.c. structure within a few hundred MD steps of imposing the rubidium potential (see Fig. 2). The cubic cell edges transformed into a rectangular parallelopiped by a decrease in the cell edge, $\vec{c}$. The particle interaction was then changed back to the Lennard-Jones. It was found that the system transformed back to the f.c.c. arrangement within a few hundred MD steps. This calculation illustrates the usefulness of the Parrinello–Rahman method for studies involving the structure–potential relationships. We have carried out an isobaric isothermal calculation employing a variable shape MC cell (*7*) and the results are indeed similar (Fig. 3).

Najafbadi and Yip (*18*) have investigated the stress–strain relationship in iron under uniaxial loading by means of a MC simulation in the isostress isothermal ensemble. At finite temperatures, a reversible b.c.c. to f.c.c. transformation occurs with hysteresis. They found that the transformation takes place by the Bain mechanism and is accompanied by sudden and uniform changes in local strain. The critical values of stress required to transform from the b.c.c. to the f.c.c. structure or vice versa are lower than those obtained from static calculations. Parrinello and Rahman (*14*) investigated the behavior of a single crystal of Ni under uniform uniaxial compressive and tensile loads and found that for uniaxial tensile loads less than a critical value, the f.c.c. Ni crystal expanded along the axis of stress reversibly.

3.2. Silver Iodide

Structural transformation in the superionic conductor silver iodide has been investigated by employing the modified molecular dynamics method in the constant-enthalpy–constant-pressure ensemble (*24*). A potential derived by considering the properties of both the β and the superionic α phases was employed for the purpose. The calculated structure, diffusion coefficient, etc., for α-AgI at 700 K were in agreement with the experiment (*25*). On cooling from 700 to 350 K, the b.c.c. lattice of iodine transformed to the close-packed h.c.p. structure accompanied by a marked decrease in D_{Ag}; the transformation was reversible on heating. Structural and dynamical properties as well as the transition temperature for the α-β transformation obtained from the MD study were in good agreement with experiment.

3.3. Molecular Crystals

Nitrogen. Nosé and Klein (*26*) carried out a MD simulation of the various phases of nitrogen using a simple Lennard-Jones 6–12 potential with $\varepsilon = 37.3$ K, $\delta = 3.31$ Å. Starting with the high-pressure room-temperature structure ($Pm3n$), results have been reported for $T = 300$ K and at lower temperatures and a presence of 70 kbar. The cell was allowed to vary in size as well as shape. Molecules in the T_d sites perform free rotation while the remaining three-quarters in D_{2d} sites rotate within a plane. Below 230 K, molecules in the D_{2d} sites align themselves parallel to the direction of the unit cell vectors while those in the T_d sites rotate almost freely. This phase has cubic symmetry ($R3c$) in which all the molecules are aligned along the same direction. The transitions were reversible.

Carbon tetrafluoride. Carbon tetrafluoride, which undergoes a transition to a plastically crystalline (orientationally disordered) phase, has been investigated by the Parrinello–Rahman molecular dynamics method under constant-pressure conditions (*6*). A simple intermolecular potential model of the Lennard-Jones form was derived by taking into account the experimen-

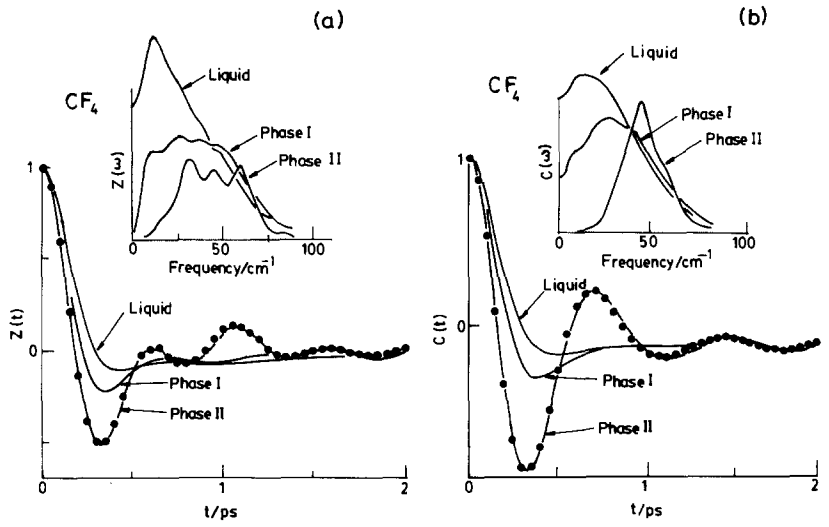

FIG. 4. (a) The velocity autocorrelation function and its power spectrum and (b) the angular velocity autocorrelation function and the power spectrum for different phases of CF_4. (From Nosé and Klein (*6*).)

tal molar volume and lattice energy. Calculations were carried out at 50.5 K and 1.2 kbar employing this potential with the starting arrangement of the ordered monoclinic phase II ($C2/c$) with $a = 8.43$, $b = 4.32$, $c = 8.48$ Å, $\beta = 120.7°$; calculations were also performed at higher temperatures and pressures. The calculated volume, lattice energy, and the r.d.f.'s of phase II were in agreement with experiment (*27*). On increasing the temperature, the system showed considerable increase in the molar volume around 75 K and the features in the radial distribution function became broad, suggesting increased molecular motion; the molecules in the lattice were orientationally disordered. The calculated change in enthalpy and molar volume were found to be in good accord with experiment (*28*). Properties of liquid carbon tetrafluoride have also been reported. Properties of solid carbon tetrafluoride have been studied by the MC method and found to be in agreement with the above results.

Time-dependent quantities have been examined (*6*) for the orientationally ordered and disordered phases as well as the liquid phases of CF_4. Power spectra for the translational and librational motions are reported (see Fig. 4). The peaks appear in the same region of frequency, suggesting strong translation–rotation coupling. The far-infrared spectrum in the ordered solid (*29*) has three peaks at 51, 57, and 66 cm^{-1}. On the basis of the significant intensity and temperature dependence of the 51-cm^{-1} band, it has been assigned to the 43-cm^{-1} band of the calculated $Z(\omega)$ and $C(\omega)$. This is a good illustration of the application of the Parrinello–Rahman MD method for the study of a crystal to plastic crystal transition. The study also shows how a simple potential can account for many of the properties exhibited by the solid. The dynamical properties seem to require a rather accurate description of intermolecular interactions. Constant-pressure and constant-volume calculations on carbon tetrafluoride (*6*) demonstrate that the single-particle dynamical properties are not very sensitive to the choice of the mass of the wall.

Bicyclo[2.2.2]octane. At low tempera-

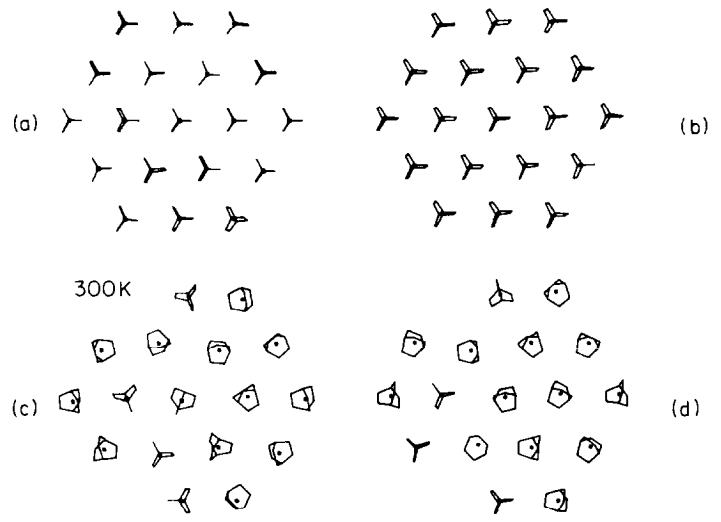

FIG. 5. A view of the bicyclo[2.2.2]octane down the trigonal axis (a) at 50 K for the 8-site model, (b) at 50 K for the 22-site model, (c) at room temperature for the 8-site model, and (d) at room temperature for the 22-site model. (From Neusy *et al.* (*32*).)

tures, bicyclo[2.2.2]octane exists as a trigonal phase with the individual molecular C_3 symmetry axes parallel to the crystal [111] directions. At 164.35 K, the ordered crystalline phase transforms to a cubic, orientationally disordered phase in which the quasi-spherical molecules exhibit increased molecular reorientation (*30, 31*). This order–disorder phase transition has been investigated by Neusy *et al.* (*32*) by means of constant-pressure MD employing two different potential models. In the first potential model of the Lennard-Jones form given by Jorgensen (*33*), each CH_2 or CH group is represented by a single interaction site and hence there are only eight interaction sites per molecule. In the model given by Williams (*34*), which is of the 6-exp form, each atom is represented by an interaction site that is placed on each atom.

Calculations carried out at 50 and 137.5 K on the ordered phase with an initial arrangement corresponding to the experimental structure (a = 6.4, c = 15.1 Å) resulted in a slightly elongated unique axis (*35*). The calculated c/a ratio was 2.6 for both the 8-site and the 22-site model as compared to the experimental value of 2.3. The molar volume determined from the 22-site model was in better agreement with experiment although the calculated molar volume was about 5% higher than the experimental value for the 8-site model. On heating to room temperature, the molecules oriented themselves almost randomly with a preference for the [111] crystallographic direction (Fig. 5). The ordered trigonal crystal was found to transform to the disordered cubic phase at about 170 K, in good agreement with experimentally determined transition temperature (164.25 K).

Power spectra of the autocorrelation functions of the linear and angular velocities parallel and perpendicular to the C_3 symmetrical axes have also been examined by Neusy *et al.* (*32*). In the rotator phase, there is good agreement with the Raman data (*36*). The calculated characteristic time (τ_4) for reorientation of the C_3 axes from one [111] direction to another and also the reorientation time (τ_3) for rotation of molecules around the C_3 axes were similar

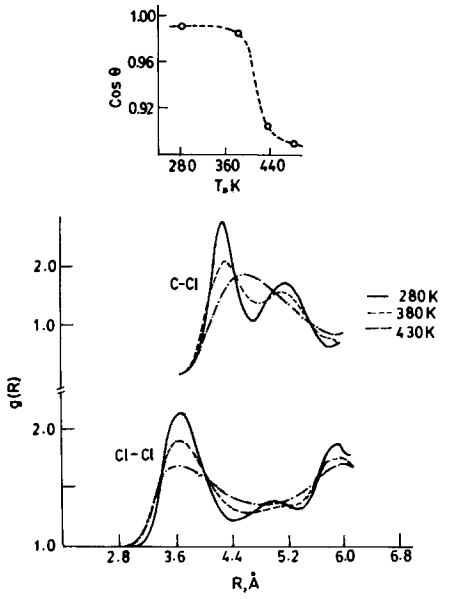

FIG. 6. Radial distribution functions C–C, C–Cl, and Cl–Cl in CCl_4 at 280, 380, and 430 K and 1.0 GPa pressure showing the changes from an ordered to an orientationally ordered phase. Inset shows a plot of cos θ against temperature. Here θ is the smallest angle between the $(\bar{a} + \bar{c})$ direction and the four Cl–Cl bonds. The dashed line is drawn to guide the eye. (From Yashonath and Rao (*19*).)

for both potential models. These results indicate that transferable intermolecular potential functions provide a reasonably good model for solids. Experimentally, from incoherent neutron scattering studies it is found that τ_4 is much slower than τ_3. It appears from these results that while simple potentials can provide a reasonable picture of the phase transitions, they cannot make detailed predictions especially with regard to the dynamics of the system.

Carbon tetrachloride. Carbon tetrachloride exists in at least five phases, Ia, Ib, II, III, and IV, of which two phases, Ia and Ib, are orientationally disordered (*37*); phases III and IV exist only at high pressures. We have carried out an investigation (*19*) of the transition from the high-pressure ordered phase III to an orientationally disordered phase by employing the generalized variable shape MC method in the isothermal isobaric ensemble. A simple Lennard-Jones potential used by McDonald *et al.* (*38*) in the simulation of liquid and solid phases with $\delta_{CC} = 4.6$ Å, $\varepsilon_{CC} = 51.2$ K, $\delta_{ClCl} = 3.5$ Å, and $\varepsilon_{ClCl} = 102.4$ K was employed in our calculations. Starting with the experimental structure (*39*) of phase III of CCl_4 with lattice parameters $a = 9.1$, $b = 5.8$, $c = 9.2$ Å and $\beta = 104.3°$, simulation was carried out at 280 K and 1.0 GPa. The calculated values of molar volume, configurational energy, lattice parameters, etc., were in agreement with the available experimental values (*39*). The r.d.f.'s for phase III are shown in Fig. 6. On increasing the temperature to 380 K, the thermodynamic properties were found to undergo small changes but, however, no significant changes were observed in the structure, the structure remaining ordered at this temperature (Fig. 7). Considerable changes in molar volume and intermolecular energy were observed on increasing the temperature to 430 K. The r.d.f.'s showed broad peaks similar to those of the liquid, suggesting increased molecular motion. The snapshot picture of the molecular arrangement in Fig. 7 shows that the crystal is orientationally disordered. This was con-

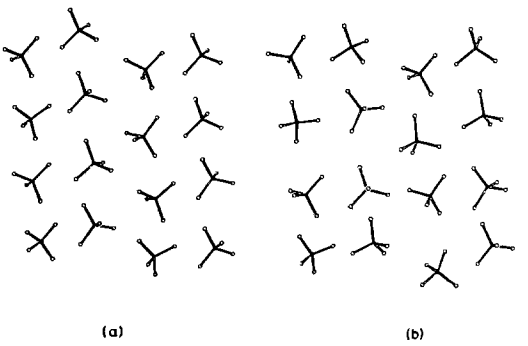

FIG. 7. A snapshot picture of the molecular arrangement viewed down the *b*-axis (a) at 380 K and (b) at 430 K in carbon tetrachloride. (From Yashonath and Rao (*19*).)

firmed by the drastic change in the minimum of the angle between the four C_3 axes of the molecule and the crystallographic [101] direction (see inset of Fig. 6). Calculations at an intermediate temperature of 405 K suggest that the transition temperature may be between 400 and 410 K, which compares well with the experimental value of 410 K (*37*).

Adamantane. Adamantane is a globular molecule in which the six methylene groups form an octahedron and the four methine groups projecting out form a tetrahedron. Adamantane exists as an ordered body-centered tetragonal solid at low temperatures (space group $P42_1c$; a = 6.6, b = 8.8 Å) (*40–42*). At 208.6 K, the solid undergoes a structural transition from the tetragonal to a cubic phase (*43*). Early X-ray studies of this phase by Nowacki (*40*) and Giocomello and Illuminati (*44*) suggested an ordered structure (space group $F43m$), but later work of Nordman and Schmitkons (*41*) showed the molecules to be orientationally disordered in the cubic phase ($Fm3m$). The nature of the high-temperature phase has, however, remained controversial (*45–47*).

We have carried out a MC simulation of adamantane in the isothermal isobaric ensemble permitting variation of the shape of the simulation cell (*48*). In these calculations, we have employed potential functions described by Jorgensen (*33*) in which there is a single interaction site for groups such as CH or CH_2. The potential parameters are, for CH_2–CH_2; ε = 0.478 kJ mole^{-1}, σ = 3.983 Å; for CH_2–CH: ε = 0.312 kJ mole^{-1}, σ = 4.118 Å; and for CH–CH: ε = 0.203 kJ mole^{-1}, σ = 4.252 Å. Calculations were carried out at 110, 213, and 298 K and atmospheric pressure. The calculated molar volume and the configurational energy are in good agreement with those from experiment (*41*). The molecules are completely ordered at 110 K and perform small librations. The CH_2–CH_2, CH–CH_2, and CH–CH r.d.f.'s (Fig. 8) show

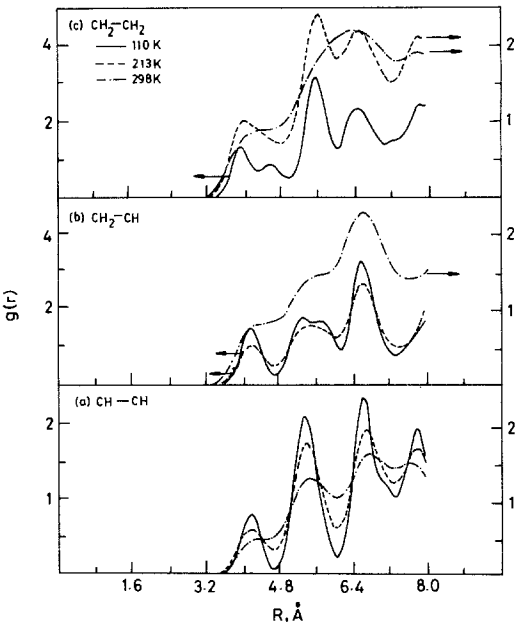

FIG. 8. Radial distribution functions for adamantane between (a) CH_2–CH_2, (b) CH_2–CH, and (c) CH_2–CH_2 groups at 110, 213, and 298 K and 1 atmosphere pressure. (From Yashonath and Rao (*48*).)

well-defined peaks at this temperature. At 213 K, the peaks become somewhat broad, but the arrangement at this temperature is still ordered. On increasing the temperature to 298 K, the r.d.f.'s show broad peaks unlike those of the ordered solid (Fig. 8). The molecules were found to perform large rotational jumps around the C_4 axis (Fig. 9). The calculated unit cell parameters are 9.31, 9.31, 9.25 Å with the angles close to 90°. These compare well with the experimental cubic cell parameter of 9.44 Å (*41*). The elongation of the c-axis on going from 213 to 298 K is also known experimentally. The calculated configurational energy (−58.0 kJ/mole) is in agreement with the heat of sublimation (−58.5 kJ/mole) (*49*). This study supports the view that the room-temperature phase of adamantane is orientationally disordered.

Biphenyl. In biphenyl, the angle between the normal to the two phenyl rings, θ,

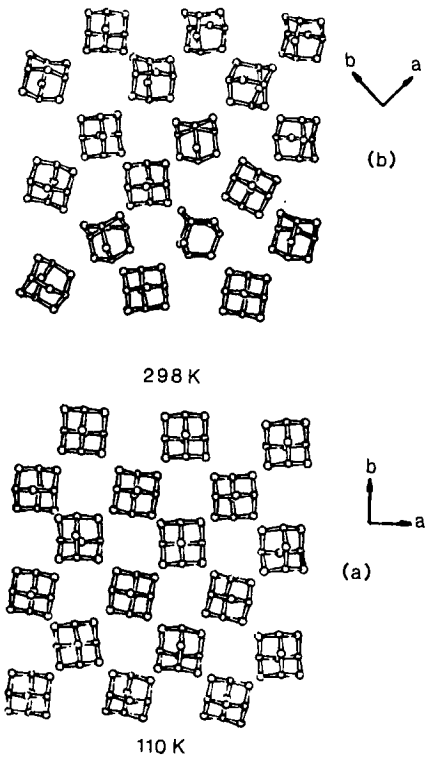

FIG. 9. A view of the instantaneous arrangement in adamantane looking down the c-axis: (a) tetragonal ordered phase at 110 K and (b) orientationally disordered cubic phase at 298 K. (From Yashonath and Rao (*48*).)

which is 42° in the vapor phase, decreases to about 32° in the melt (*50*). Upon cooling, the melt crystallizes in the space group $P2_1/a$, where the two phenyl rings are essentially planar. Further cooling results in a phase with the two rings deviating from this planar arrangement. Raman spectroscopic and other studies indicate that this solid–solid phase transformation is a second-order transition occurring over a range of temperatures (75 to 40 K) (*50, 52*). The conformations in the vapor and the liquid phases result from a balance between resonance stabilization and ortho–ortho hydrogen repulsion. In the solid, intermolecular interactions also play a very significant role and hence packing considerations lead to a planar conformation in the high-temperature solid phase (*53*). We have carried out some preliminary MC investigations on this interesting solid by employing a 6-exp atom–atom potential derived by Misskaya *et al.* (*54*) and used by Ramdas and Thomas (*55*) in their study of the structure of *p*-terphenyl. The same potential was used to calculate the intermolecular interactions as well as the intramolecular interactions arising out of ortho–ortho hydrogen repulsions. The potential parameters were

$$A_{CC} = 1761.9 \text{ kJ A}^6 \text{ mole}^{-1};$$
$$B_{CC} = 299{,}646 \text{ kJ mole}^{-1};$$
$$C_{CC} = 3.68 \text{ Å}^{-1};$$
$$A_{CH} = 493.8 \text{ kJ A}^6 \text{ mole}^{-1};$$
$$B_{CH} = 77{,}841 \text{ kJ mole}^{-1};$$
$$C_{CH} = 3.94 \text{ Å}^{-1};$$
$$A_{HH} = 121.4 \text{ kJ A}^6 \text{ mole}^{-1};$$
$$B_{HH} = 20{,}506.5 \text{ kJ mole}^{-1};$$
$$C_{HH} = 4.29 \text{ Å}^{-1}.$$

The initial arrangement was the experimental structure of the high-temperature phase with $a = 7.82$, $b = 5.58$, $c = 9.44$ Å and $\beta = 94.6°$ (*51*). The calculated intermolecular energy at 110 K was −68.2 kJ mole^{-1} compared to the sublimation energy of −81.6 kJ mole^{-1}. The average angle between the two phenyl rings was 20° as against the experimentally observed planar conformation (*51*). The discrepancy in the observed angle could be due to the large repulsion in the region of 1.8–2.2 Å in the hydrogen–hydrogen interaction potential functions. Potential functions were derived by considering the lattice energy of aromatic hydrocarbons such as benzene, naphthalene, etc., where only intermolecular distances larger than 2.2 Å are present (*54*). It is, therefore, not surprising that the potential may not represent the interactions correctly at lower distances even though it may show excellent agreement at larger distances. A recent calculation on *n*-butane

has shown that the conformational angle is much more sensitive to the potential than other properties (*56*). On cooling the solid to 40 K, we found that θ increased to 25.3° with significant decrease in libration around the long molecular axis. This trend is in agreement with experiment (*57*). We plan to carry out further calculations using a different potential model where the intermolecular interactions and intramolecular interactions are modelled by different potential functions. These calculations are expected to answer several questions, especially those concerning the distribution of the interplanar angle, the structure of the low-temperature solid, and the nature of the motion in the high-temperature phase.

4. Glasses

Computer simulation has contributed significantly to the understanding of equilibrium and dynamic properties of supercooled liquids and glasses. Hard-sphere, Lennard-Jones, and ionic glasses have been studied (*58–61*), providing some insights into structural and other aspects (*62, 63*). For example, it has been found that the split second peak, a characteristic feature of the r.d.f.'s of metallic glasses, is observed in computer-simulated Lennard-Jones glasses (*62*). The MD method was limited to the microcanonical ensemble in these studies until the constant-temperature and constant-pressure MD was introduced by Andersen. The constant-volume and energy conditions used in the earlier studies did not permit direct comparison with the laboratory glasses, where the conditions of preparation of glasses are very different (*64, 65*). Also, some of the typical characteristics of laboratory glasses were absent in computer-simulated glasses (*64*). The smeared nature of the transition at temperatures which are higher than the experimental transition temperature prompted Angell and co-workers (*64, 65*) to suggest that the transition observed in computer simulation studies bears little resemblance to laboratory glasses. More recent results obtained under isothermal- isobaric conditions by MC and MD methods indicate that there is, in fact, a close parallel between the laboratory and the computer-simulated glasses. The quenching rates employed in computer simulation are, however, orders of magnitude higher than those employed in the laboratory and, as a consequence, computer-simulated glasses differ in certain aspects from those obtained in the laboratory. Frenkel and McTague (*66*) have reviewed the earlier studies in this area. We shall limit the present discussion to certain significant findings based on some of the recent studies on monatomic, molecular, and orientational glasses.

Lennard-Jones glass. Extensive calculations on a monatomic Lennard-Jones argon-like system have been carried out by Fox and Andersen (*67*) under conditions of constant temperature and constant pressure with a variety of cooling rates. These workers have reported density, enthalpy, and self-diffusion coefficient at different pressures and temperatures. The glass transition temperature obtained from the density–temperature plot is essentially identical to that obtained from the enthalpy–temperature plots. The glass transition temperature is higher at higher pressures. Also the slower the rate of cooling, the higher was the density of the glass, indicating the existence of slow relaxation processes involving volume changes (see Fig. 10). The apparent self-diffusion coefficient could be fitted equally well to both Arrhenius and Doolittle equations. Interestingly, the pressure dependence of the structural relaxation was different from that of self-diffusion. Hysteresis in the transition was evident from a comparison of the heating and the cooling runs.

The above results indicate that even though the quenching rates employed in

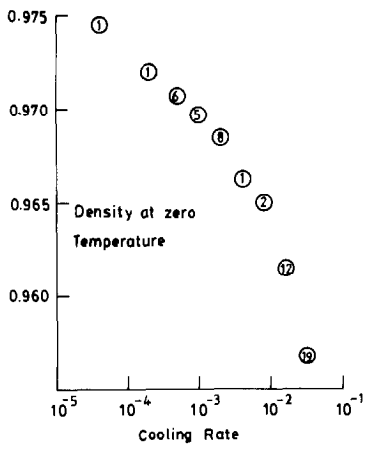

FIG. 10. The densities obtained at different cooling rates at $T = 0$ and $p = 1$ for the Lennard-Jones glass. The cooling rate is the value of the stochastic collision frequency per particle, ν. The number of runs employed to obtain the reported average is shown inside each point. (From Fox and Andersen (*67*).)

computer simulation are very high, the general features of simulated glasses are quite similar to those of laboratory glasses. The demonstration of the history dependence of the properties and also the presence of hysteresis near the transition are significant. The radial distribution functions for glasses obtained by employing two different cooling rates shown in Fig. 11 are indeed similar; the r.d.f.'s are somewhat insensitive to the structural changes taking place in the glass. Our calculations on methane (*68*) in which only orientational degrees of freedom were permitted, however, show distinct changes in the r.d.f.'s of the glass before and after annealing (see Fig. 12). This is the only study that we are aware of that shows changes in r.d.f.'s even though it is for an orientationally disordered glass and not for a positionally disordered glass. This is probably because barriers for going from one state to another state are much smaller in the case of orientational glass. The history dependence of the properties of the glass has also been observed in a study on isopentane glass (*69*); the intermolecular energy of the glass is lowered by a small amount on annealing near the glass transition.

Isopentane glass. A recent MC simulation of isopentane glass (*70*) using realistic potentials has yielded some insight into glass structure and the nature of rearrangement occurring during the glass transition. Isothermal isobaric ensemble calculations have been performed on glasses obtained by instantaneous quenching of the liquid. There are four distinct groups in isopentane: CH, CH_2, the methyl group attached to CH, $CHCH_3^*$, and the methyl group attached to CH_2, $CH_2CH_3^*$. These give rise to ten r.d.f.'s. Four of these r.d.f.'s, between the somewhat inaccessible CH and other groups (referred to as the i-type r.d.f.'s), are similar in nature. They have a single peak within the 9-Å region at a somewhat larger distance of 5.3 to 6.2 Å. The remaining six r.d.f.'s (the p-type r.d.f.'s) in the liquid between the peripheral groups CH_2, $CH_2CH_3^*$, and $CHCH_3^*$ show a shoulder around 4 Å and a main peak around 6 Å. A

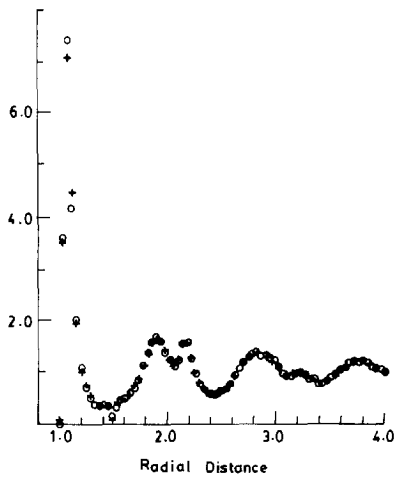

FIG. 11. Radial distribution functions for systems obtained by continuous cooling at $p = 1$. The stochastic collision frequencies were 3.2 for the + and 0.04 for the O points. (From Fox and Andersen (*67*).)

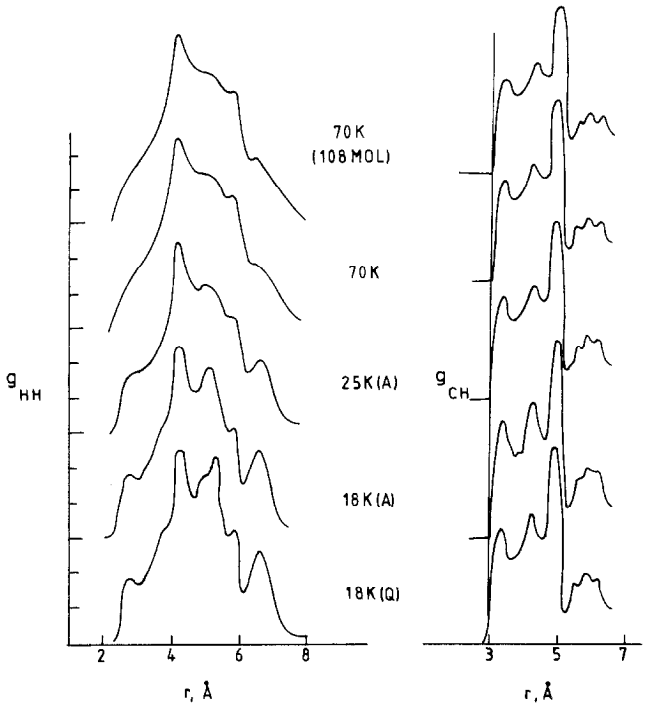

FIG. 12. Pair distribution functions $g_{HH}(r)$ and $g_{CH}(r)$ for the plastic and annealed (A) and quenched phases (Q) of methane. Only the orientational degrees of freedom were considered in the calculation. Note the distinct change in the r.d.f.'s in $g_{HH}(r)$ and to a smaller extent of $g_{CH}(r)$ on annealing. (From Yashonath and Rao (*68*).)

few typical r.d.f.'s are shown in Fig. 13. On cooling below the glass transition temperature, peaks generally become sharper and show more features. However, there are several interesting differences between the i-type and the p-type r.d.f.'s. While the

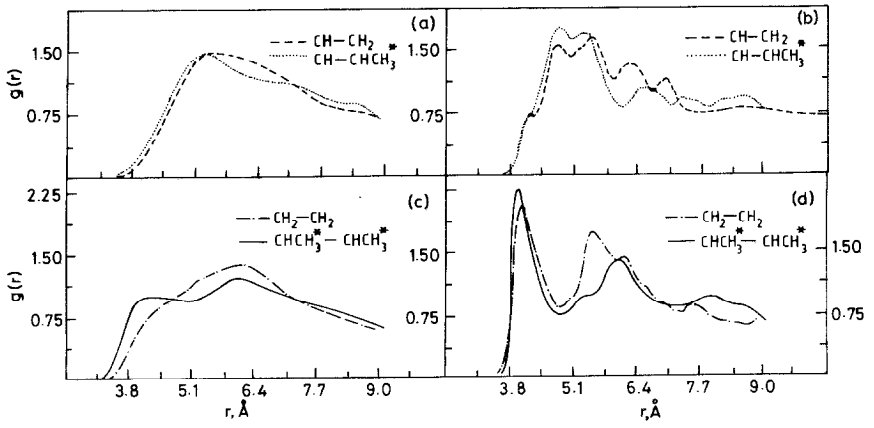

FIG. 13. Typical r.d.f.'s (i-type) between the inaccessible CH and other groups (a) for liquid isopentane at 301 K and (b) for the glass at 30 K. Typical r.d.f.'s (p-type) between the peripheral groups (c) for the liquid at 301 K and (d) for the glass at 30 K. (From Yashonath and Rao (*70*).)

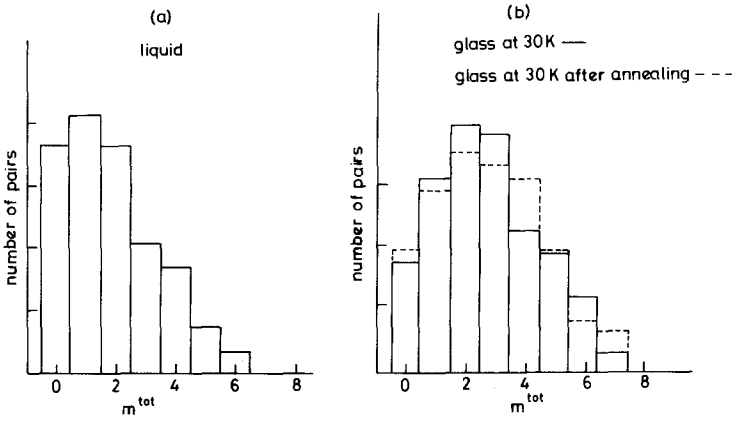

FIG. 14. Histograms for the distribution of the number of pairs of neighbors, in arbitrary units, for different values of m_{tot} for (a) isopentane liquid at 301 K and (b) glass at 30 K, with and without annealing. (From Yashonath and Rao (*71*).)

peak positions of the i-type r.d.f.'s are shifted towards lower distances, those of p-type r.d.f.'s do not show such shifts. This is surprising as one would have expected a more or less uniform shift of peaks in all the r.d.f.'s towards lower distances on vitrification. Furthermore, on glass formation, the shoulder in the p-type r.d.f.'s of the liquid around 4.2 Å gains significantly in intensity as compared to the main peak. These observations suggest the existence of a somewhat complex rearrangement of the neighbors. This rearrangement seems to involve the shift of the center of mass of the neighbors towards each other. In addition, the disproportionate increase in the first peak intensity on vitrification and the absence of shift towards lower distances for the p-type r.d.f.'s suggests the presence of a molecular reorientational mechanism.

The number of pairs of neighbors specified in arbitrary units is plotted against m_{tot}, where m_{tot} is the sum of the number of groups in the region of the first peak (for the six p-type r.d.f.'s), in Fig. 14 for the liquid at 301 K and the glass at 30 K; the effect of annealing the glass is also shown in the figure. The shift of the histogram towards higher values of m_{tot} indicates the overall increase in the number of neighbors in the region of the first peak. We have been able to estimate the reorientational contribution E_r^g to the increase in energy from the r.d.f.'s and find the reorientational contribution to the increase in the intermolecular energy on vitrification (*71*) to be nearly 50%. In obtaining an estimate of E_r^g we have neglected the reorientational contribution from the i-type r.d.f.'s and made the assumption that the p-type r.d.f.'s of the hypothetical glass are similar to those of the liquid but for the increased intensity due to the higher density. In other words,

$$g_h(r) = g_l(r) n_t^g / n_t^l, \tag{15}$$

where the $g_h(r)$ and $g_l(r)$ are the r.d.f.'s of the hypothetical glass and the liquid respectively and n_t^g and n_t^l are the total number of neighbors within a distance of 9 Å for the glass and the liquid.

The total intermolecular energy, E_{inter}, and the total reorientational contribution, E_r, are plotted against temperature in Fig. 15 for isopentane cooled from 301 K to 220, 120, 50, 40, and 30 K. The change in slope observed around 80 K is considerably more

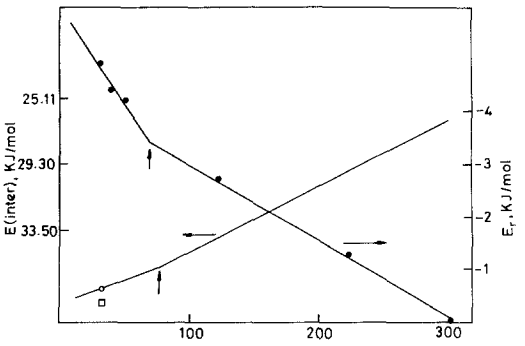

FIG. 15. Variation of the total intermolecular energy, E_{inter}, and the contribution from reorientation, E_r, for isopentane at different temperatures obtained by instantaneous cooling from 301 K. (From Yashonath and Rao (*70, 71*).)

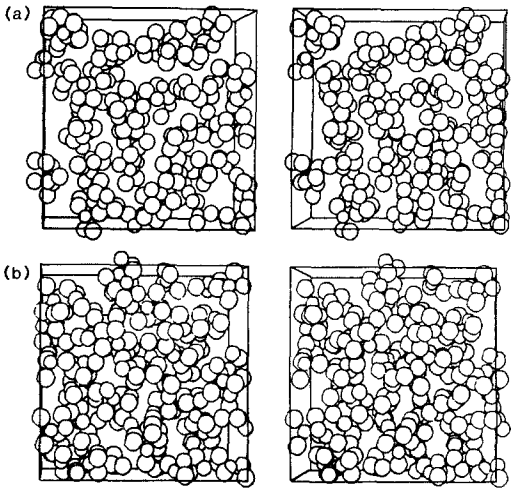

FIG. 16. Stereoplots showing the structure (a) in the liquid at 301 K and (b) in the glass at 30 K for isopentane. Note that the molecules at the surface interact with those at the opposite surface. (From Yashonath and Rao (*70*).)

marked in the case of E_r as compared to E_{inter}. It appears, therefore, that the reorientational mechanism contributes significantly to the changes in properties near the glass transition. We have also found that significant structural rearrangements involving orientational degrees of freedom occur on annealing the glass. Stereoplots of the molecular arrangement in the liquid and the glass are shown in Fig. 16. The presence of considerable free volume even in the glass is evident from this figure.

Investigations into the properties of glassy water and methanol are presently in progress in our laboratory. Whether amorphous solid water exhibits a glass transition is an aspect of considerable interest (*72*). Preliminary studies (*73*) indicate that liquid water quenched to low temperatures does indeed show a glass transition, with the nature of species, intermolecular energy, heat capacity, etc., showing the expected changes at the transition temperature (Fig. 17).

5. Concluding Remarks

The generalized MD and MC methods can be used for studying different classes of materials and phenomena. The method introduced by Parrinello and Rahman (*5*) permits one to derive interparticle potentials taking into account more than one phase of

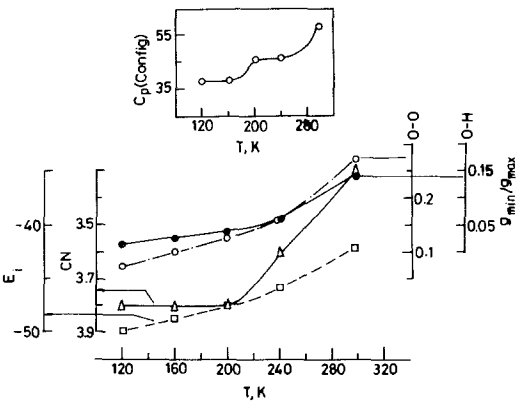

FIG. 17. Temperature variation of internal energy. E_i (kJ mole^{-1}), coordination number (CN), and g_{min}/g_{max} ratios of water showing the occurrence of the glass transition in the 200–240 K range. Volume also shows a similar change, but a slightly lower temperature. In the inset, variation of the configurational heat capacity, C_p (J deg^{-1} mole^{-1}), with temperature is shown. (From Chandrasekhar and Rao (*73*).)

the solid. These potentials are expected to be more accurate and to describe the solid over a wider range of temperatures and pressures. The new MD and MC methods provide a very useful means of studying a variety of solids. Study of different phases of elemental solids by these methods would be interesting. Such studies would, however, be limited by the availability of pair potentials. Recently, there has been an attempt to derive pair potentials for metals like sodium, magnesium, and aluminum (*74*). Phase transitions in molecular crystals such as benzene and *p*-dichlorobenzene should provide insight into the microscopic behavior in these solids and be useful in interpreting the large amount of experimental data available in the literature. The mechanism of transitions and the dependence of transition temperature and other properties on the intermolecular potential can be fruitfully investigated. In our opinion, systematic studies of orientationally disordered solids (see Refs. (*75–77*) for the very recent papers) as well as matrix isolated molecular systems such as CH_4 in Ar matrix should be worthwhile. The liquid crystalline state can be effectively investigated by MC and MD methods. Yet another interesting area would be to investigate the effect of defects on the phase transitions and other properties of solids. The above simulation methods could be very profitably employed in the area of "crystal engineering" and organic solid-state reactions as well as in the study of the liquid crystalline state. If the interaction potentials are known accurately, they could also be used in deriving the crystal structures of simple solids at finite temperatures.

Acknowledgments

The authors thank the Department of Science and Technology and the University Grants Commission for support of this research.

References

1. M. L. KLEIN, *Annu. Rev. Phys. Chem.* **36,** 525 (1985).
2. N. METROPOLIS, A. W. ROSENBLUTH, M. N. ROSENBLUTH, A. H. TELLER, AND E. TELLER, *J. Chem. Phys.* **21,** 1087 (1953).
3. B. J. ALDER AND T. W. WAINWRIGHT, *J. Chem. Phys.* **31,** 459 (1959).
4. H. C. ANDERSEN, *J. Chem. Phys.* **72,** 2384 (1980).
5. M. PARRINELLO AND A. RAHMAN, *Phys. Rev. Lett.* **45,** 1196 (1980).
6. S. NOSÉ AND M. L. KLEIN, *Mol. Phys.* **50,** 1055 (1983); *J. Chem. Phys.* **78,** 6928 (1983).
7. S. YASHONATH AND C. N. R. RAO, *Mol. Phys.* **54,** 245 (1985).
8. (a) W. W. WOOD, *in* "Physics of Simple Liquids" (H. N. V. Temperley, J. S. Rowlinson, and G. S. Rushbrooke, Eds.), North-Holland, Amsterdam (1968); (b) J. P. VALLEAU AND S. G. WHITTINGTON, *in* "Statistical Mechanics, Part A: Equilibrium Techniques" (B. J. Berne, Ed.), p. 137, Plenum, New York (1977); (c) J. P. VALLEAU AND G. M. TORRIE, *ibid.*, p. 169; (d) J. J. ERPENBECK AND W. W. WOOD, *in* "Statistical Mechanics, Part B: Time-Dependent Processes" (B. J. Berne, Ed.), p. 1, Plenum, New York, (1977); (e) J. KUSHICK AND B. J. BERNE, *ibid.*, p. 41; (f) K. BINDER (Ed.), "Monte Carlo Methods," Methuen, London (1964); (g) K. BINDER (Ed.), "Monte Carlo Methods in Statistical Physics," Springer-Verlag, New York (1979).
9. J. M. HAILE AND H. W. GRABEN, *J. Chem. Phys.* **73,** 2412 (1980).
10. H. TANAKA, K. NAKANISHI, AND N. WATANABE, *J. Chem. Phys.* **78,** 2626 (1983).
11. S. NOSÉ, *Mol. Phys.* **52,** 255 (1984); *J. Chem. Phys.* **81,** 511 (1984).
12. D. J. EVANS, *J. Chem. Phys.* **78,** 3297 (1983).
13. J. M. HAILE AND S. GUPTA, *J. Chem. Phys.* **79,** 3067 (1983).
14. M. PARRINELLO AND A. RAHMAN, *J. Appl. Phys.* **52,** 7182 (1981).
15. M. PARRINELLO AND A. RAHMAN, *J. Chem. Phys.* **76,** 2622 (1982).
16. J. R. RAY AND A. RAHMAN, *J. Chem. Phys.* **80,** 4423 (1984).
17. J. R. RAY AND A. RAHMAN, *J. Chem. Phys.* **82,** 4243 (1985).
18. R. NAJAFBADI AND S. YIP, *Scr. Metall.* **17,** 1199 (1983).
19. S. YASHONATH AND C. N. R. RAO, *Chem. Phys. Lett.* **119,** 22 (1985).
20. M. PARRINELLO AND A. RAHMAN, *in* "Melting, Localization and Chaos" (R. K. Kalia and P. Vashishta, Eds.), Elsevier, Amsterdam/New York (1982).

21. S. YASHONATH, Ph.D. thesis, Indian Institute of Science, Bangalore, India (1985).
22. G. S. PAWLEY AND G. W. THOMAS, *Phys. Rev. Lett.* **48,** 410 (1982).
23. G. S. PAWLEY, *J. Mol. Struct.* **30,** 17 (1985).
24. M. PARRINELLO, A. RAHMAN, AND P. VASHISHTA, *Phys. Rev. Lett.* **50,** 1073 (1983).
25. W. ANDREONI AND J. C. PHILLIPS, *Phys. Rev. B* **23,** 6456 (1981).
26. S. NOSÉ AND M. L. KLEIN, *Phys. Rev. Lett.* **50,** 1207 (1983).
27. C. N. BOL'SHUTKIN, V. M. GASAN, A. I. PROKHAVTILOV, AND A. I. ERENBURG, *Acta Crystallogr., Sect. B* **28,** 3542 (1972).
28. J. W. STEWART AND R. I. LAROCK, *J. Chem. Phys.* **28,** 3542 (1972).
29. Y. A. SATATY, A. RON, AND F. H. HERBSTEIN, *J. Chem. Phys.* **62,** 1094 (1975).
30. J. N. SHERWOOD (Ed.), "The Plastically Crystalline State," Wiley, New York (1979); C. N. R. RAO, *Proc. Indian Acad. Sci. (Chem. Sci.)* **94,** 181 (1985).
31. E. F. WESTRUM, JR., W. K. WONG, AND E. MORAWETZ, *J. Phys. Chem.* **74,** 2542 (1970).
32. E. NEUSY, S. NOSÉ, AND M. L. KLEIN, *Mol. Phys.* **52,** 269 (1984).
33. W. L. JORGENSEN, *J. Amer. Chem. Soc.* **103,** 335 (1981).
34. D. E. WILLIAMS, *J. Chem. Phys.* **47,** 4680 (1967).
35. A. J. LEADBETTER, J. PIPER, R. M. RICHARDSON, AND P. G. WRIGHTON, *J. Phys. C* **15,** 5921 (1982).
36. J. L. SAUVAJOL, Thesis, Universite de Lille (1983).
37. R. G. ROSS AND P. ANDERSON, *Mol. Phys.* **36,** 39 (1978).
38. I. R. MCDONALD, D. G. BOUNDS, AND M. L. KLEIN, *Mol. Phys.* **45,** 521 (1982).
39. G. J. PIERMARINI AND A. B. BRAUN, *J. Chem. Phys.* **58,** 1974 (1973).
40. W. NOWACKI, *Helv. Chim.* **28,** 1283 (1945).
41. C. E. NORDMAN AND D. L. SCHMITKONS, *Acta Crystallogr.* **18,** 764 (1965).
42. J. DONOHUE AND S. H. GOODMAN, *Acta Crystallogr.* **22,** 352 (1967).
43. S. C. CHANG AND E. F. WESTRUM, *J. Phys. Chem.* **64,** 1547 (1960).
44. G. GIOCOMELLO AND G. ILLUMINATI, *Gazz. Chim. Ital.* **75,** 246 (1945).
45. P. A. REYNOLDS, *Acta Crystallogr., Sect. A* **34,** 362 (1978).
46. J. P. AMOUREUX, M. BEE, AND J-C. DAMIEN, *Acta Crystallogr., Sect. B* **36,** 2633 (1980).
47. P. A. REYNOLDS AND B. R. MARKEY, *Acta Crystallogr., Sect. A* **35,** 627 (1979).
48. S. YASHONATH AND C. N. R. RAO, *J. Phys. Chem.* **90,** 2552 (1986).
49. R. J. JOCHEMS, *Chem. Thermodyn.* **14,** 395 (1982).
50. A. M. PONTE GONCALVES, *Prog. Solid State Chem.* **13,** 1 (1980).
51. G. P. CHARBONNEAU AND Y. DELUGEARD, *Acta Crystallogr., Sect. B* **32,** 1420 (1976).
52. R. M. HOCHSTRASSER, G. W. SCOTT, A. H. ZEWAIL, AND H. F. FUESS, *Chem. Phys.* **11,** 273 (1975); C. A. HUTCHINSON, JR., AND V. H. MCCANN, *J. Chem. Phys.* **61,** 820 (1974).
53. G. CASALONE, C. MARIANI, A. MUGNOLI, AND M. SIMONETTA, *Mol. Phys.* **15,** 339 (1968).
54. K. V. MISSKAYA, I. E. KOZLOVA, AND V. F. BEREZNITSKAYA, *Phys. Status Solidi B* **62,** 291 (1974).
55. S. RAMDAS AND J. M. THOMAS, *J. Chem. Soc., Faraday Trans. 2* **72,** 1251 (1976).
56. A. BANBN, F. SERRANO ADAN, AND J. SANTAMERIA, *J. Chem. Phys.* **83,** 297 (1985).
57. A. S. CULLICK AND R. E. GERKIN, *Chem. Phys.* **23,** 217 (1977).
58. L. V. WOODCOCK, *Ann. N.Y. Acad. Sci.* **371,** 274 (1981).
59. J. H. R. CLARKE, *J. Chem. Soc., Faraday Trans. 2* **75,** 1371 (1979).
60. S. BREWER AND M. J. BISHOP, *J. Chem. Phys.* **75,** 3522 (1981).
61. L. V. WOODCOCK, C. A. ANGELL, AND P. CHEESMAN, *J. Chem. Phys.* **65,** 1656 (1976).
62. F. F. ABRAHAM, *J. Chem. Phys.* **72,** 359 (1980).
63. J. R. FOX AND H. C. ANDERSEN, *Ann. N.Y. Acad. Sci.* **371,** 123 (1981).
64. C. A. ANGELL, J-H-R. CLARKE, AND L. V. WOODCOCK, *Adv. Chem. Phys.* **48,** 397 (1981).
65. C. A. ANGELL, *Ann. N.Y. Acad. Sci.* **371,** 136 (1981).
66. D. FRENKEL AND J. P. MCTAGUE, *Annu. Rev. Phys. Chem.* **31,** 491 (1980).
67. J. R. FOX AND H. C. ANDERSEN, *J. Phys. Chem.* **88,** 4019 (1984).
68. S. YASHONATH AND C. N. R. RAO, *Chem. Phys. Lett.* **101,** 524 (1983).
69. S. YASHONATH, K. J. RAO, AND C. N. R. RAO, *Phys. Rev. B* **31,** 3196 (1985).
70. S. YASHONATH AND C. N. R. RAO, *Proc. R. Soc. London, Ser. A* **400,** 61 (1985).
71. S. YASHONATH AND C. N. R. RAO, *J. Phys. Chem.* **90,** 2581 (1986).
72. S. R. ELLIOTT, C. N. R. RAO, AND J. M. THOMAS, *Angew Chem. Int. Ed.* (English) **25,** 31 (1986).
73. J. CHANDRASEKHAR AND C. N. R. RAO, *Chem. Phys. Lett.*, in press.
74. D. G. PETTIFER AND M. A. WARD, *Solid State Commun.* **49,** 291 (1984).
75. R. D. MOUNTAIN AND A. C. BROWN, *J. Chem. Phys.* **82,** 4236 (1985).
76. M. FERRORIO, I. R. MCDONALD, AND M. L. KLEIN, *J. Chem. Phys.* **83,** 4726 (1985).
77. R. W. IMPEY, M. L. KLEIN, AND I. R. MCDONALD, *J. Chem. Phys.* **82,** 4690 (1985).